J. Fluid Mech. (1987), *vol.* 182, *pp.* 85–109
Printed in Great Britain

Organized structures in a compressible, turbulent boundary layer

By ERIC F. SPINA AND ALEXANDER J. SMITS
Gas Dynamics Laboratory, Department of Mechanical and Aerospace Engineering, Princeton University, Princeton, NJ 08544, USA

(Received 17 July 1986)

Experimental results are presented that show the existence of organized structures in a compressible, turbulent boundary layer. Results were obtained using arrays of hot wires and wall pressure transducers in a Mach-3 zero-pressure-gradient boundary layer. The VITA method of conditional sampling was used to deduce average pressure events at the wall and mass flux events throughout the boundary layer; these results show qualitative similarity to those found in incompressible flows. By conditioning upon the middle hot wire from a three-wire probe, evidence is found suggesting that structures exist of a height comparable with the boundary-layer thickness. Furthermore, two-point conditional sampling was used to show that an average pressure event could be extracted by conditioning upon mass-flux events. From this procedure we found that the structures maintain their shape as they travel downstream and also that their spanwise extent is very limited.

The inferred angle from correlations between two hot wires, and between a hot wire and a wall-pressure transducer, indicate that the average structure is inclined at approximately 45° for a large part of the boundary layer. This result agrees well with structures observed in schlieren photographs of supersonic boundary layers. Measurements of the instantaneous angle show a wide distribution of structure angles, and the general behaviour of the large-scale structures is consistent with the hairpin loop model of wall turbulence.

1. Introduction

This paper is one of a series describing the behaviour of supersonic turbulent boundary layers (see, for example, Jayaram, Taylor & Smits 1987; Smits & Muck 1987). In the previous work, Reynolds-averaged turbulent stresses were measured to investigate shock-wave/boundary-layer interactions, and to study the effects of bulk compression and concave surface curvature. The present study is different in two respects. First, the flow under investigation is the undisturbed flat plate, zero-pressure-gradient boundary layer which served as the initial condition for the earlier studies. Secondly, the measurements are designed to improve our understanding of the large-scale, time-dependent motions in the boundary layer, rather than to examine the time-averaged behaviour.

The primary aim of this study is to explore the differences between the structure of subsonic and supersonic equilibrium boundary layers. According to Morkovin (1962), the dynamics of compressible turbulent shear layers follow the incompressible pattern closely, as long as the fluctuating Mach numbers remain small. Together with the assumption that the fluctuating velocity field is solenoidal, this hypothesis forms the basis of virtually all modelling schemes.

However, it is well known that the spreading rate of a free-shear layer decreases significantly with Mach number (see, for example, Bradshaw's report in Kline, Cantwell & Lilley 1981). There also exists some evidence (Owen, Horstmann & Kussoy 1975) that the intermittency profile at high supersonic Mach numbers is fuller than the corresponding subsonic profile. It is possible that the density gradients in a supersonic shear layer affect the large-scale structure and that there exists a damping effect of Mach number on the turbulent motions which may be important for wall turbulence. It would not be surprising to find differences between compressible and incompressible boundary layers since the vorticity transport equation describes the transport of vorticity per unit mass, rather than the absolute vorticity. Density gradients must therefore affect the vorticity dynamics to some extent, and the extent of this influence will vary with Mach number. In contrast, the success of the van Driest transformation in scaling mean velocity profiles over a wide range of Mach numbers (see, for example, Fernholz & Finley 1980) argues against the presence of significant compressibility effects in equilibrium layers. In any case, the available evidence is not conclusive, and further work seems desirable.

In particular, studies of compressible-boundary-layer structure seem to be desirable since previous research on large-scale boundary-layer structure has been almost exclusively confined to incompressible flows (Robinson 1985; Moin & Kim 1985; Thomas & Bull 1983; Subramanian *et al.* 1982; Rajagopalan & Antonia 1979; Chen & Blackwelder 1978; Brown & Thomas 1977). That work has indicated the presence of a complex hierarchy of organized motions. Of particular note are the observations by Head & Bandyopadhyay (1981) who used flow visualization to study a zero-pressure-gradient boundary layer over a wide range of Reynolds numbers ($500 < Re_\theta < 17500$). They found that 'hairpin' vortices, first observed in connection with the near-wall bursting process (Kline *et al.* 1967; Offen & Kline 1974, 1975; Smith 1984), may extend throughout the boundary layer. The layer appeared to consist of hairpin eddies 'attached' to the wall region, inclined to the wall at a characteristic 'eddy angle' of 40–50°. Instead of merely controlling the production and diffusion of turbulent energy (as with bursting), the structures observed by Head & Bandyopadhyay appear to describe the whole of the boundary layer. In many ways, however, their structures are similar to those used by Smith and others to model the bursting phenomenon.

Some evidence also exists for the presence of coherent motions in supersonic flows. For example, the schlieren photographs of Deckker & Weekes (1976) and Deckker (1980) show the floor of a duct after the passage of a shock wave (see Head & Bandyopadhyay 1981). For two different shock strengths, 45° striations were visible close to the wall. Similar structures are shown in two shadowgraphs published by Van Dyke (1982), reproduced here as figure 1(*a*, *b*). The photographs show turbulent boundary layers on slender bodies of revolution moving at Mach numbers of 1.84 and 2.58 respectively. Large-scale motions inclined at about 45° can be clearly seen in these close-ups. The effect of optical integration is reduced in these flows owing to the use of bodies of revolution; still, no information on the spanwise extent of the structures can be inferred from the photographs.

Despite this flow-visualization evidence, the quantitative study of turbulent-boundary-layer structure in compressible flows has been largely neglected. Owen & Horstman (1972) made extensive space–time correlation measurements in a hypersonic boundary layer, focusing on mean convection velocities. More recently, Robinson (1986) reported average structure-angle measurements from a supersonic flow which bore a resemblance to those found in several incompressible flows.

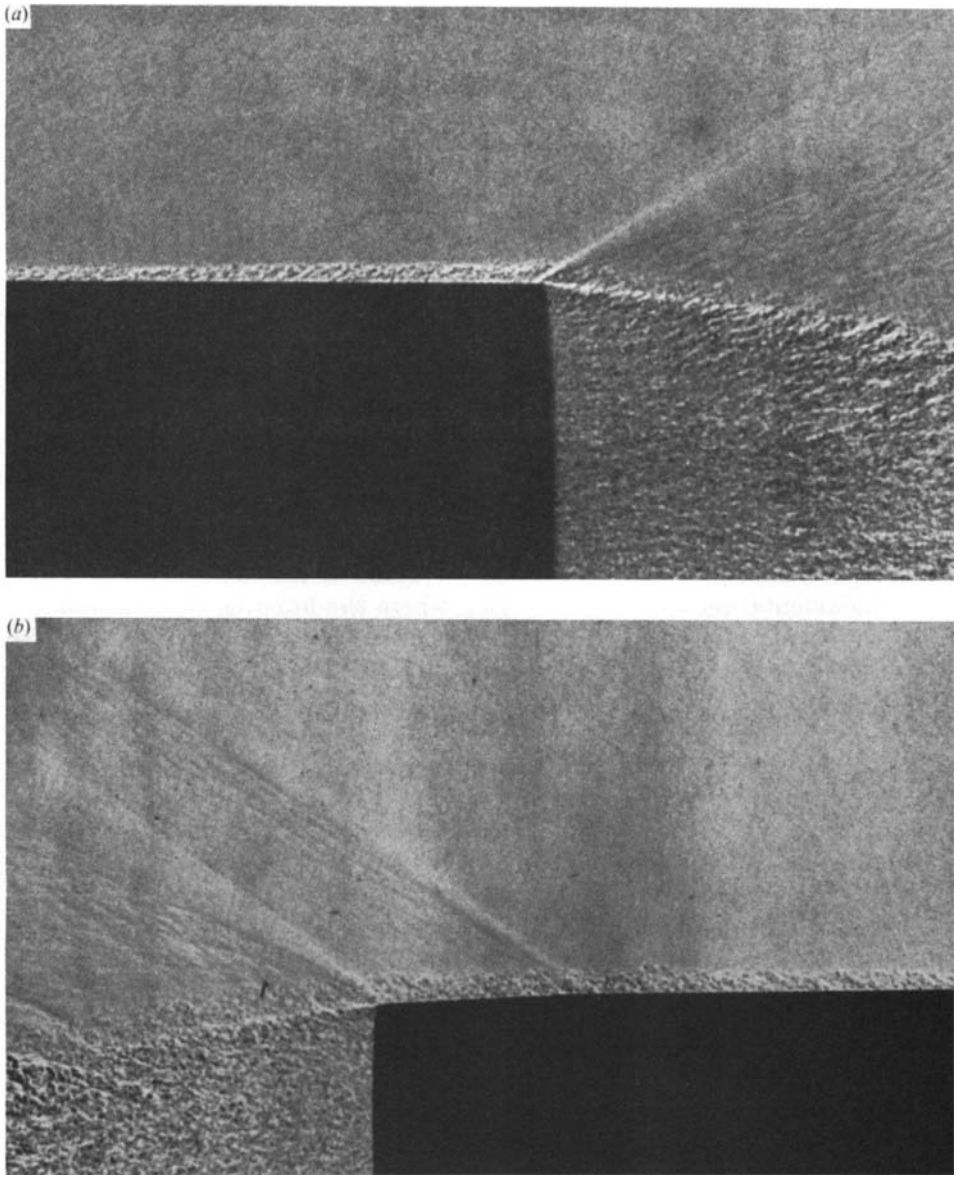

FIGURE 1. Structures inclined at approximately 45° can be seen in these shadowgraphs of boundary layers over axisymmetric bodies-of-revolution (details from photographs taken by A. C. Charters – Van Dyke 1982). The flow is from left to right and the Mach number at the edge of the layer is approximately (*a*) 1.8 and (*b*) 2.5.

Comparisons will be made between the present study and Robinson's where appropriate. No measurements describing the instantaneous structure exist in compressible flow, and much remains to be learned about their size, shape and extent of influence. The present study aims to provide some of the first measurements of this kind.

Turbulent fluctuations were recorded at several locations simultaneously, providing spatial and temporal information about the structures. Constant-temperature hot-wire anemometry was used, and at high overheat ratios the output is proportional

M_∞	2.87
Re_∞/m	6.5×10^7
δ	28 mm
δ^*	6.2 mm
U_∞	565 m/s
$(\rho u)_\infty$	479 kg/m^2 s
P_{wall}	3.34 p.s.i.
C_f	0.00114

TABLE 1. Flow conditions on the tunnel centreline at $x = 2.21$ m

to fluctuations in mass flux (Smits, Hayakawa & Muck 1983). Since the correlation between density and velocity fluctuations is about 0.8 (Dussauge & Gaviglio 1981), the mass-flux signal is approximately proportional to either density or streamwise velocity fluctuations. Conditional sampling was used to deduce both the mean and instantaneous behaviour of the large-scale structure. Prior to the conditioning of the signals, a complete time-series analysis was performed, including cross-correlations and cross-spectra. The measurements were confined to the outer layer of this flow for two fundamental reasons: (i) the region where the bursting process occurs was too small to be resolved (the minimum y^+ value was about 650), and (ii) the time-scale needed to identify the bursting process ($10\nu/u_\tau^2$) was too small to be resolved with the available instrumentation.

Although the character of the outer-layer structure strongly suggests that the bursting process is intimately involved in its development, it was not possible to link the two phenomena owing to the aforementioned factors. Therefore the words 'event', 'organized structure', 'organized motion', 'large-scale structure' will refer to the outer-layer motions that were studied; while the word 'burst' will refer exclusively to the bursting process in the inner portion of the boundary layer.

The equipment, instrumentation, experimental techniques and data reduction methods are described in §2. An overview of the boundary layer, including mean flow measurements is given in §3. The two-point correlation results are discussed in §4 and the conditional-sampling results in §5. Section 6 presents the final discussion and conclusions.

2. Instrumentation and techniques

The experimental studies were performed in the Princeton University 200 mm × 200 mm high-Reynolds-number, supersonic, blowdown wind tunnel. For all tests the stagnation pressure was 6.9×10^5 N/m$^2 \pm 0.5\%$ and the stagnation temperature was nominally 270 K. The flow had a free-stream Mach number of 2.87 (± 0.01) with a unit Reynolds number of 6.5×10^7/m ($\pm 4\%$). The walls were approximately adiabatic and the free-stream turbulence level was 1–1.5 %. The test boundary layer developed on the tunnel floor, and the measurements were centred around a point 2210 mm downstream of the throat. The boundary-layer thickness at that point was 28 mm, where δ was defined as the point where the mass flow reached 99 % of its free-stream value. Flow conditions are given in table 1.

For the mean-flow surveys, the data acquisition system consisted of a Hewlett-Packard 1000 minicomputer, and a Preston Scientific GMAD-4 analog-to-digital converter with a maximum sampling frequency of 50 kHz. For the fluctuating-data

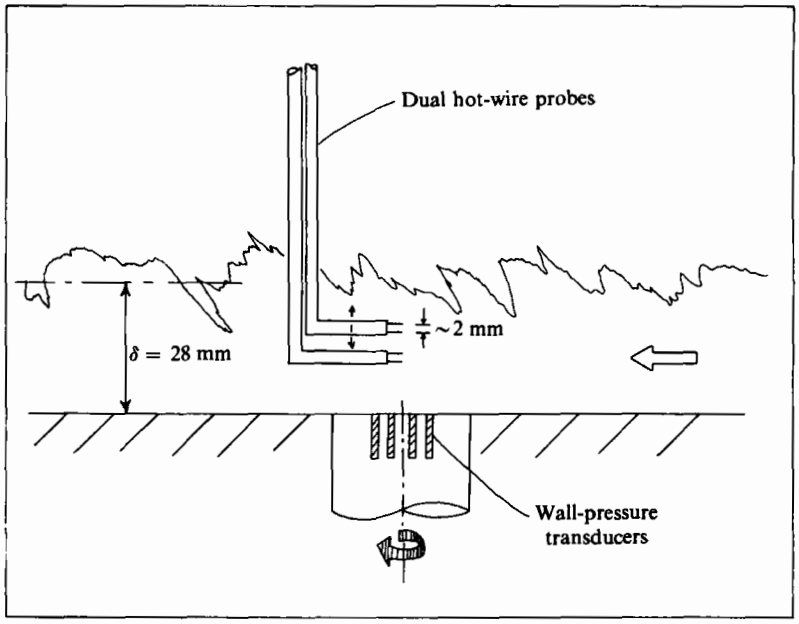

FIGURE 2. Arrangement of four hot-wire probes with four wall-pressure transducers.

collection, a much faster system was used, consisting of a VAX 11/750 minicomputer and LeCroy CAMAC data acquisition units. Simultaneous sampling rates up to 1 MHz on each of four channels were possible, with a continuous record length of 24576 data points per channel.

Measurements of the wall-pressure fluctuations were made using four identical miniature differential pressure transducers manufactured by Kulite Semiconductor Products Inc. Each transducer had a 0.71 mm diameter silicon sensing element on which a fully active Wheatstone bridge was bonded atomically. The natural frequency, as quoted by the manufacturer, was 500 KHz. The transducers were mounted in-line in a cylindrical plug (see figure 2), which was then fitted in the test-section floor. The separation distance between each transducer was 5.1 mm, and the transducers were located symmetrically about the centre of the plug. The plug could be rotated through 360°, yawing the transducers relative to the flow.

Hanly (1975) has shown that the flushness of the transducers is an important parameter in measuring fluctuating surface pressure accurately. Accordingly, the transducers were adjusted to less than 0.05 mm under the floor surface using a microscope.

The signals were band-pass filtered by Ithaco analog filters. The high-pass was set to 250 Hz to reduce electronic noise and low-frequency tunnel noise, and the low-pass was set to 125 KHz to reduce the effect of resonance. The Kulite spectra showed that the resonance frequency was located at 480 KHz. In addition to that spike, however, other abnormalities were found in the spectra all the way down to 40 KHz. The energy distribution, seen in figure 3, shows the effect of these transducer resonances.

The energy is expected to fall off monotonically with frequency after reaching its peak value near 10 kHz; however, additional spikes are seen at the same frequencies that had exhibited electronic resonance during noise tests. Evidently these had been amplified by the flow, making the spectrum beyond 40 kHz inaccurate. Most of the

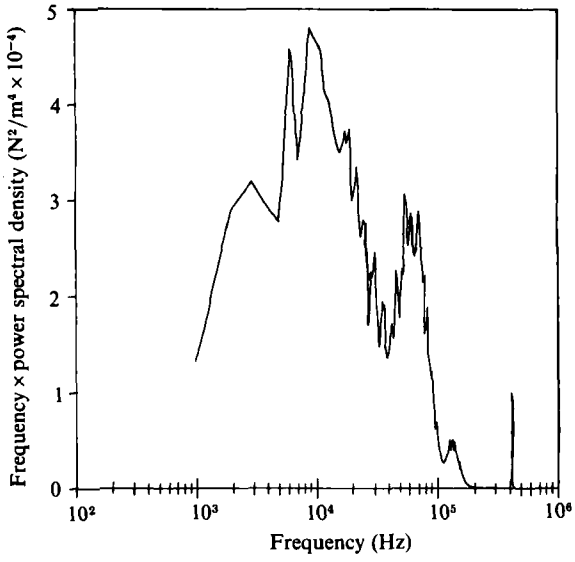

FIGURE 3. Typical measured wall-pressure energy distribution.

energy of the wall-pressure fluctuations appears to be contained at lower frequencies, but since the pressure signals were used for relative comparisons, the response was considered to be adequate.

DISA 55M10 constant-temperature hot-wire anemometers were used to measure the instantaneous mass flux. The hot-wire probes were constructed by electroplating 5 μm diameter tungsten wire with copper and soft soldering the wire onto the probe prongs (2.5–3 mm separation). The wires were then etched using a dilute sulphuric acid solution to expose an active portion of tungsten wire 0.8–1.0 mm in length. A small amount of slack was introduced into the active length of the wire to avoid strain gauging at high frequencies. This type of probe, first recommended by Kovasznay (1950) and recently analysed by Smits *et al.* (1983), gives reasonable wire lifetimes, minimizes interference from bow shocks emanating from the prongs, and yields a reasonable frequency response.

A small Mach-3 pilot tunnel was used to calibrate the wires and adjust their frequency response. An acceptance criterion for each wire was that the upper roll-off frequency be at least 120 KHz.

The spatial resolution of the hot-wire probe, even for streamwise fluctuations, is determined by the active length of the wire, and it restricts the frequencies that can be discerned. Since the active portion is larger than the smallest turbulence scales, the hot wire distorts the contribution of the high-frequency end of the spectrum. Wyngaard (1968) suggested that the measured value of the one-dimensional spectra falls to one-half of its value at a wavenumber of $2.1/L$ (where L is the active length of the wire). Under test conditions, for a length of 0.8 mm, this wavenumber corresponds to a frequency of 250 KHz. The most restrictive constraint on the hot-wire response is therefore not the spatial filtering effect, but the roll-off frequency of the anemometer.

The fluctuating component of each anemometer signal was band-pass filtered from 10 Hz to 500 KHz. The total instantaneous values of the mass flux were found by adding the mean voltage to the fluctuating voltage and inverting the calibration

curve directly, thereby avoiding the use of the linearized sensitivity coefficients. The instantaneous values of the mass-flux fluctuations were then obtained by subtracting the time-averaged mass flux from the total instantaneous mass flux.

For multi-wire runs, a special hot-wire support was designed to hold four normal wires in two pairs, one pair above the other, and the two pairs of wires could be moved relative to each other vertically (see figure 2). No data was actually taken using all four wires; however, runs were made using both two and three hot wires simultaneously. In these cases the wire separation distances ranged from $0.09y/\delta$ to $0.21y/\delta$.

By combining the use of wall-pressure transducers and hot wires, simultaneous measurements of the instantaneous wall pressure and instantaneous mass flux were made. The hot wires were placed at different points in the flow (relative to the wall-pressure transducers) to obtain a wide spatial resolution of the flow field.

Phase shifts between signals must be avoided to obtain accurate correlation measurements. In multi-wire runs, the hot-wire anemometers were all identical DISA 55M10 systems and the wires were only used if they had similar frequency responses. Hence, the relative phase shift through the frequency range of interest was minimized. Recent results taken by E. M. Fernando (private communication) in the same boundary layer using hot wires with a frequency response better than 250 kHz have substantiated all the conclusions given in this paper.

Correlations between the signals from a pressure transducer and a hot wire were accurate only at frequencies where both systems have negligible phase shift; that is, the correlations are accurate only below 40 kHz.

3. Preliminary results

Prior to taking turbulence measurements, mean-flow surveys were taken in the floor boundary layer. Previous surveys of the same tunnel-floor boundary layer (Settles 1975; Taylor 1984; Jayaram *et al.* 1987) showed that the flow was typical of a high-Reynolds-number, well-developed turbulent boundary layer, with an extensive logarithmic region and a wake factor of 0.5, and a shape factor of 1.2. To measure the spanwise and longitudinal variations in static pressure, a 100 mm spanwise (z-direction) region and a 200 mm streamwise (x-direction) region were surveyed. The maximum peak-to-peak spanwise variation was less than 5%. The streamwise survey revealed a peak-to-peak variation of 6% (corresponding to 1.4% variations in Mach number) and a slight adverse pressure gradient. The pressure gradient was caused by the growth of the displacement thickness, and it was considered small enough to be neglected.

To investigate the two-dimensionality, two spanwise Pitot pressure surveys were taken at two different positions, $y/\delta = 0.14$ and 0.36 mm. A 10% variation in Pitot pressure was observed. This three-dimensionality is most probably due to the constriction of the sidewall boundary layers through the converging–diverging nozzle; however, for the purpose of studying the boundary-layer structure, these effects may not be too significant and they were discounted in this study.

The turbulence measurements were analysed by using two-point correlation methods and conditional sampling. Each analysis will now be considered in turn.

4. Two-point correlation results and discussion

A full time-series analysis, including spectral analysis, was performed on all combinations of the measured fluctuations: pressure–pressure, pressure–mass flux, and mass flux–mass flux. Only those results that contribute to the main conclusions are presented here; the remainder can be found in Spina & Smits (1986).

4.1. *Mass flux–mass flux results*

Two hot wires, one directly above the other at a fixed separation distance of $\xi/\delta = 0.09$, were traversed through the boundary layer. The calculated space–time correlations at different distances from the wall are shown in figure 4. The peak values of the correlations are quite high, reaching a maximum of 0.65 near the middle of the boundary layer. More importantly, the dimensionless delay time ($\tau^* = \tau U_\infty/\delta$) corresponding to the peak of the space–time correlation $\tau^*_{\max}$, decreases from 0.4 ($\tau = 20\ \mu\text{s} \pm 0.5$) at the floor to nearly zero at the edge of the boundary layer.

The high peak level of the correlation and the non-zero value of the time delay imply that both wires are detecting the same 'disturbance', and that one wire is detecting it before the other. Since the time shift was applied to the upper wire, the peak at negative τ^* means that the upper wire detects the disturbance first; i.e. the disturbance leans downstream. Accordingly, an angle θ can be defined for this 'front' by using the value of $\tau_{\max}$ along with the wire separation distance ξ and the local mean velocity: that is,

$$\theta = \tan^{-1}\left[\frac{\xi}{\bar{U}\tau_{\max}}\right].$$

Strictly speaking, the local streamwise convection velocity should be used to determine this angle (Robinson 1986; Brown & Thomas 1977), but the convection velocity has not been determined for this flow. However, the difference in the mean structure angle owing to small variations in the convection velocity is small, and therefore the average velocity was used here.

The angle θ may be called an 'average structure angle', in that it is associated with an average large-scale motion. The results from three different traverses can be seen in figure 5 as a function of position in the boundary layer. At the midpoint of the boundary layer the resolution of the time shift corresponds to an angular uncertainty of $\pm 3°$. The angle is small near the floor, increases quickly to about 45°, and it remains constant at this value throughout 70% of the boundary layer. Finally, the angle shows a rapid increase at the edge of the boundary layer. Note that the distribution of the structure angle seems to be independent of the two different separation distances chosen.

The distribution of θ is in accordance with Head & Bandyopadhyay's (1981) observations in a subsonic boundary layer at lower Reynolds numbers. They observed hairpin loops which displayed small angles near the floor and 45° through the central portion of the boundary layer, followed by a slight increase near the edge. While the present study traverses two 'detection probes' through the boundary layer at a fixed separation distance (small compared to δ), most other measurements of this kind have used one detection probe (whether it is a hot wire, shear-stress gauge, etc.) fixed at the wall and another probe that was traversed through the boundary layer, thereby varying the separation distance. The fixed-separation method used here results in a typical mean structure angle of 45°, while the variable-separation method seems to

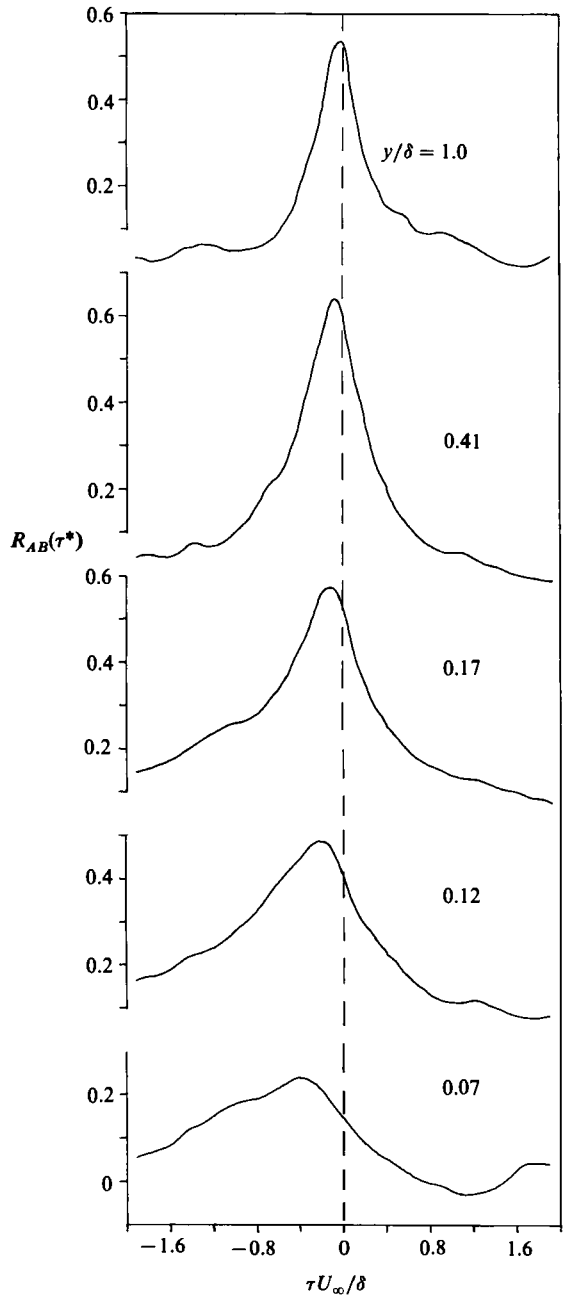

FIGURE 4. The space–time correlation of mass-flux fluctuations throughout the boundary layer. Hot-wire separation is 0.09δ.

give a lower characteristic value; in supersonic flow Robinson (1986) found 30° and in incompressible flows Brown & Thomas (1977) found 18°, whereas Rajagopalan & Antonia (1979) found 12.5°, and Robinson (1985) found 16°. The advantage of the present method is that the slope of the structure is determined locally, instead of being inferred from a large-scale measurement.

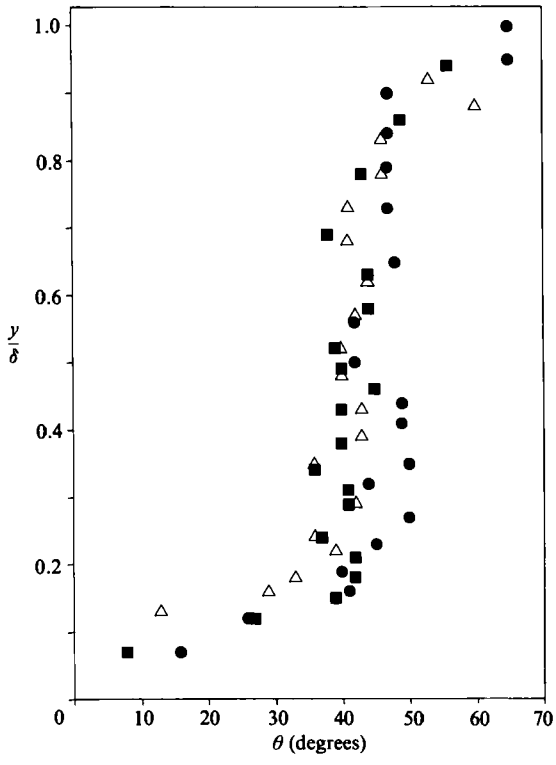

FIGURE 5. Computed large-scale structure angle throughout the boundary layer for different wire-separation distances. ●, $\xi/\delta = 0.08$; ■, $\xi/\delta = 0.09$; △, $\xi/\delta = 0.21$.

4.2. *Pressure–mass flux results*

Cross-correlations were computed between pressure fluctuations at the wall and mass-flux fluctuations measured at various points within the boundary layer. Figure 6 shows the correlations with the hot wire located 0.13δ above the pressure transducer for several different streamwise and spanwise separations. For these correlations the time shift was applied to the pressure signal; therefore, for streamwise separations, a peak at positive time shift implies a downstream-leaning structure.

The first point of interest is the rather low level of correlation, with a maximum peak of 0.2 for even the smallest transducer separations. This low correlation is due in part to the difference in frequency content of the pressure and mass-flux signals, and because pressure waves are not convected with the flow. The results are still useful for comparisons, however, and it will be seen that they can be enhanced through conditional sampling.

A streamwise separation of 0.91δ does not change the strength and shape of the correlation, indicating that the structures retain their shape and coherence as they convect downstream. In contrast, when a spanwise separation is introduced between the hot wire and pressure transducer, the correlation decreases significantly for a separation of 0.11δ and completely disappears with a separation of 0.45δ. The structures appear to have a very limited spanwise extent. A statement can now be made about the structures seen in the shadowgraphs of figure 1. The shadowgraph integrates across the entire flow field; thus the structures, which seem to be of limited spanwise extent, must have very high gradients to be clearly visible.

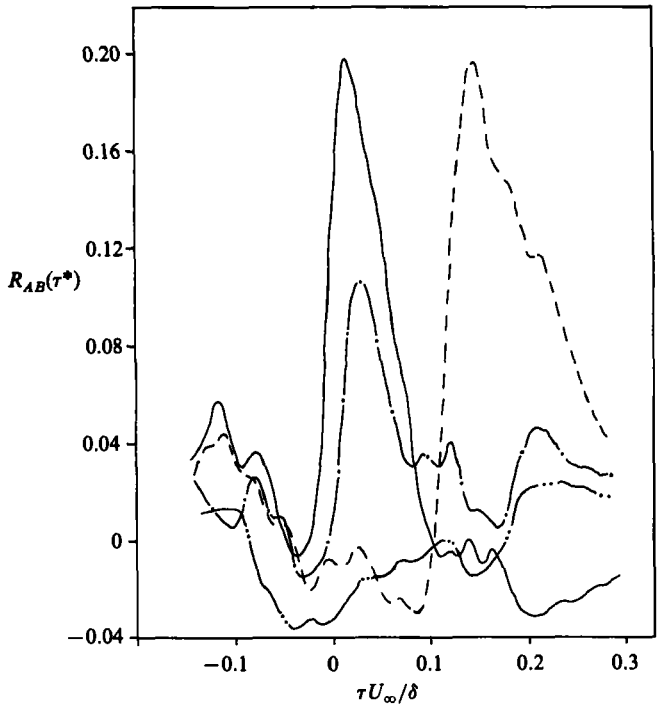

FIGURE 6. Space–time correlation between a wall-pressure signal and a mass-flux signal at $y/\delta = 0.13$ for various transducer separations: ——, $\Delta x/\delta = 0$, $\Delta z/\delta = 0$; – – – –, $\Delta x/\delta = 0.91$, $\Delta z/\delta = 0$; —·—, $\Delta x/\delta = 0.09$, $\Delta z/\delta = 0.11$; —··—, $\Delta x/\delta = 0.09$, $\Delta z/\delta = 0.45$.

5. Conditional-sampling results and discussion

The time-averaged measurements given in §4 showed the presence of 45° structures similar to the structures observed by some researchers in subsonic flows at low Reynolds number. Conditional-sampling techniques were used to further investigate the structure of these organized motions and to gain an understanding of their instantaneous behaviour. The conditional-sampling technique allows special consideration to be given to segments of the signal where certain conditions are fulfilled. The total number of consecutive points satisfying these conditions make up an 'event'. If these 'events' are carefully chosen, it is assumed that they represent particular fluid-dynamic phenomena; that is, they are the signature of characteristic structures.

Two types of conditional sampling were used, one-point and two-point. In one-point conditional sampling, the same signal is processed twice; once to define the conditions under which averaging will occur (detection) and once to actually average over the detected events (averaging). In two-point conditional sampling, the detection and averaging are done upon signals acquired at different spatial locations. Two-point conditional sampling, therefore, allows time- and lengthscales of the events to be explored.

The VITA technique, first developed by Blackwelder & Kaplan (1976), was used for the conditional sampling. This technique uses the intermittent character of the short-time variance of the detection signal to detect common patterns in the boundary layer. It is designed so that peaks in the short-time variance signal

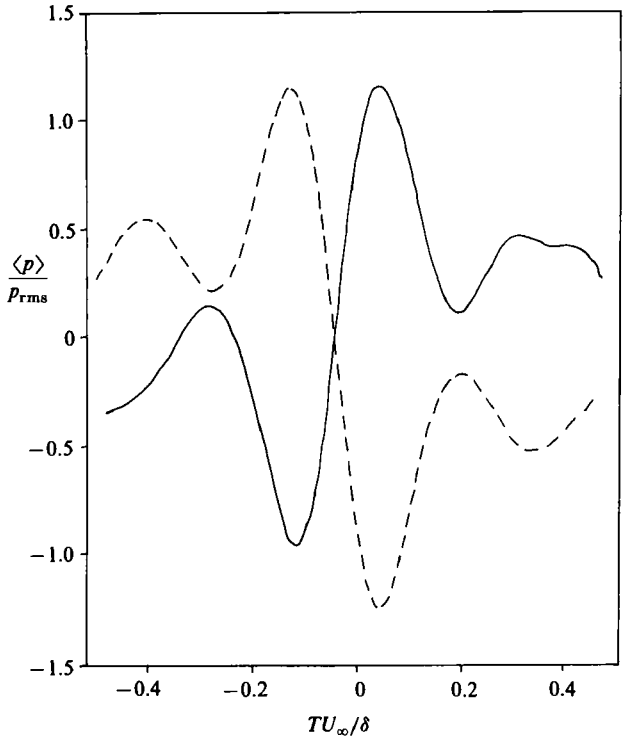

FIGURE 7. 'Optimized' average VITA pressure events: ——, positive; – – –, negative.

correspond to regions of higher turbulent activity and therefore indicate the existence of organized structures.

The details of the VITA technique will not be repeated here; the reader is referred to the original paper, Blackwelder & Kaplan (1976), and to Johansson & Alfredsson (1982). Its basis is the comparison of the short-time-averaged variance of a turbulent signal to its long-time-averaged variance. When this ratio exceeds a preset threshold, an 'event' is detected. The events are then classified as either positive or negative depending upon the slope of the signal at the centre of the event. A conditional average can be computed using the midpoint of the events as a reference point.

There are two degrees of freedom in the VITA technique: the period of the short-time variance and the level of the threshold. Because of this, the physical interpretation of peaks in the short-time variance has been a subject of much discussion (Subramanian *et al.* 1982; Bogard & Tiederman 1986; Johansson & Alfredsson 1982). Despite its shortcomings the technique can still be used as a basis for comparing subsonic and supersonic flows. The structure of incompressible boundary layers has been characterized in a number of investigations using the VITA technique, and a comparison with the structures deduced from this compressible flow is readily possible. Furthermore, it will be seen that the shape and extent of the average structures determined by cross-correlation methods can also be deduced from the ensemble-averaged events detected by the VITA method of conditional sampling.

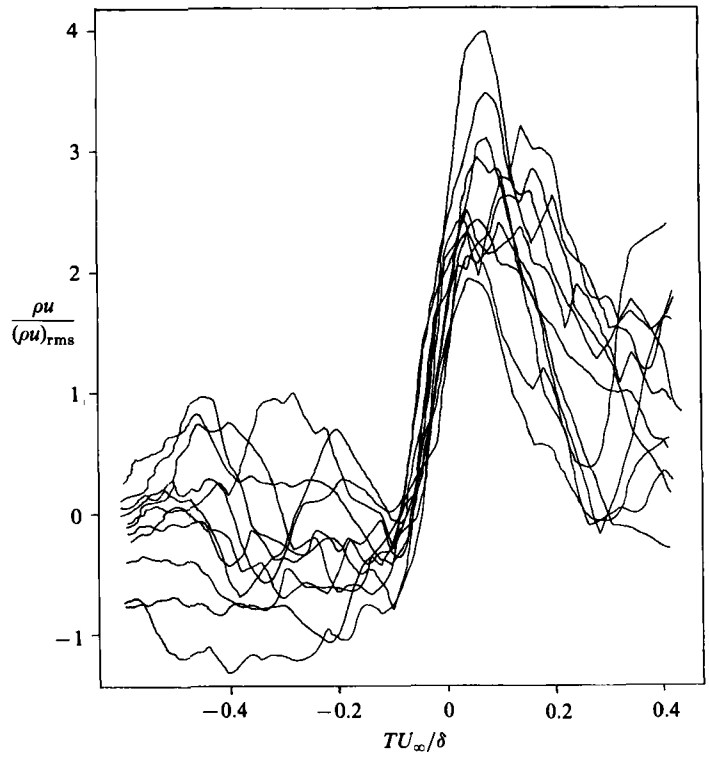

FIGURE 8. Superimposed individual positive mass-flux events at $y/\delta = 0.03$, $T^*_{\rm ST} = 0.2$, $k = 0.8$.

5.1. *One-point pressure*

The wall pressure was conditioned upon itself using the VITA technique. Here, detection and sampling occurred at the same spatial location. The threshold and dimensionless short-time-variance period ($T^*_{\rm ST} = T_{\rm ST}\, U_\infty/\delta$) were chosen to give the most energetic average event while retaining a significant number of realizations. The average positive and negative wall-pressure events, seen in figure 7, were detected with a threshold k of 0.8 and $T^*_{\rm ST} = 0.2$. From peak to peak the average positive event was 2.2 times the pressure r.m.s. level, while the average negative event was 2.5 times the r.m.s. level.

The significant features of the average events are: (i) the very sharp rise or fall about which the event is centred; (ii) the elevated pressure level after the positive event and the decreased pressure level after the negative event; and (iii) the dip in the positive event before the steep rise and the rise in the negative event before the sharp fall. The inverse symmetry of the average events suggests that the positive and negative events are not independent; rather, it appears as if the negative event immediately follows the positive event to form one single peak. This will be seen to be the case in §5.3 when the pressure event is derived by conditioning on the mass-flux signal.

5.2. *One-point mass flux*

The VITA technique was used to condition the streamwise mass-flux signal at several points throughout the boundary layer. Initially only one hot wire was used, so that detection and sampling occurred at the same spatial location.

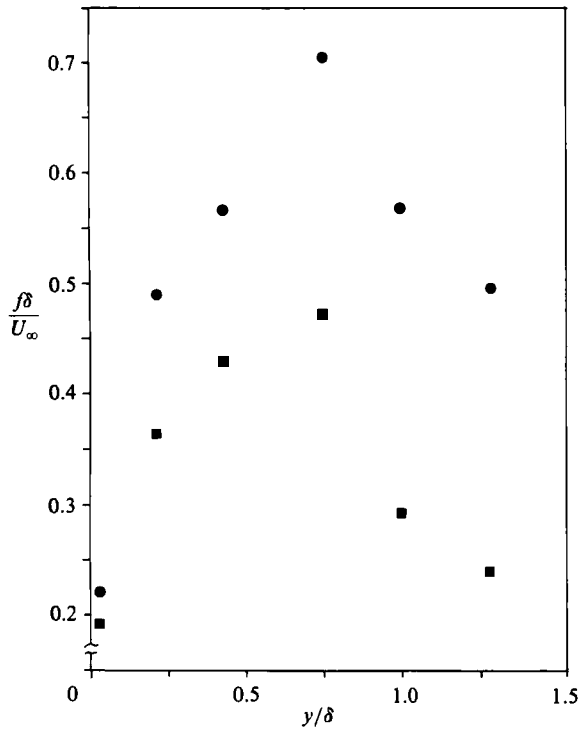

FIGURE 9. Frequency of mass-flux events as a function of position in the boundary layer: ■, positive events; ●, total events; $T^*_{ST} = 0.2$, $k = 0.8$.

Before examining the results, we need to consider the effect of the sampling criteria on the nature of the deduced positive and negative mass-flux events.

In figure 8 a number of individual positive mass-flux events are shown for a y/δ value of 0.03 ($y^+ = 650$) with $T^*_{ST} = 0.2$ and a threshold of 0.8. The similarity of the events along the steep velocity rise and the uniformity in width of the peaks is particularly striking.

Three interesting trends appear in figure 9, which shows the dimensionless frequency ($f^* = f\delta/U_\infty$) of positive events and total events (positive plus negative) against position in the boundary layer for a fixed set of detection parameters. First, as expected, the frequency of events decreases as the edge of the boundary layer is approached. Lower-frequency (larger) motions are expected in the outer regions of the boundary layer, and therefore fewer events will be detected. Also, no events occur in the free stream, so a drop-off is imperative.

Secondly, the number of total events and positive events falls off drastically near the wall. This is caused by the band-pass-filter characteristics of the short-time variance, with the inverse of the short-time-variance period being the centre frequency (Johansson & Alfredsson 1982). With a hierarchical structure of frequencies in the boundary layer, fewer events will be detected near the floor since the frequencies of the most prevalent structures will be too high to contribute to the short-time variance.

Thirdly, the total events near the floor consist almost exclusively of positive events, while further from the wall the split between positive and negative events becomes more equal. Again referring to the hierarchical structure of the boundary layer, it

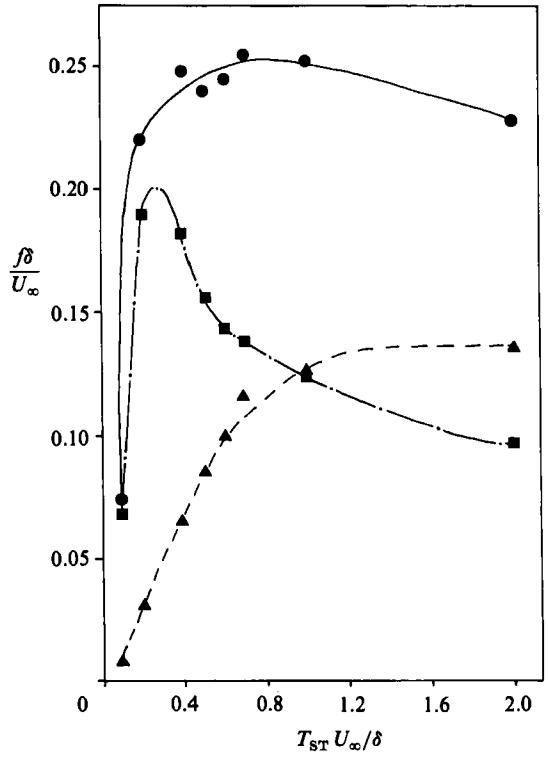

FIGURE 10. Frequency of mass-flux events as a function of short-time-variance period at $y/\delta = 0.3$: ■, positive events; ▲, negative events; ●, total events; threshold = 0.8.

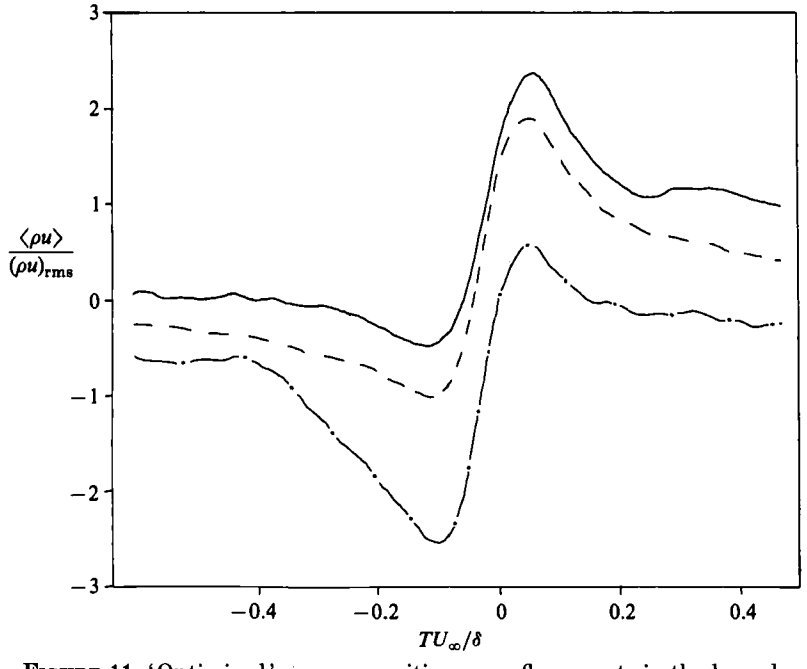

FIGURE 11. 'Optimized' average positive mass-flux events in the boundary layer: ——, $y/\delta = 0.03$; – – – –, 0.43; —·—, 1.0; $T^*_{ST} = 0.2$, $k = 0.8$.

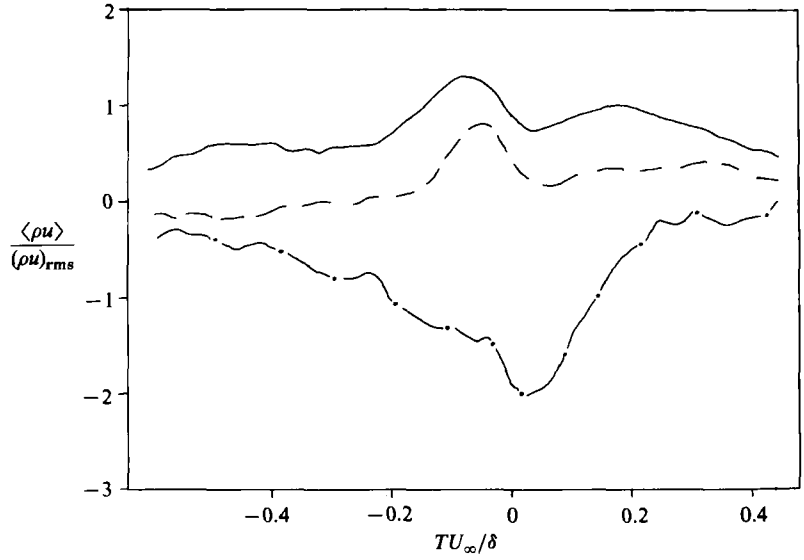

FIGURE 12. 'Optimized' average negative mass-flux events in the boundary layer: ——, $y/\delta = 0.03$; – – –, 0.43; —·—, 1.0; $T^*_{\rm ST} = 1.0$, $k = 0.8$.

would appear that the negative events have a lower-frequency content. Since there are fewer low-frequency structures near the wall, the number of negative events detected there will be less than that detected elsewhere. This explanation is supported by the results given in figure 10, which shows the frequency of total events, positive events, and negative events versus the short-time-variance period for the station nearest the floor. We see that the number of negative events increases as the short-time-variance period increases. Again, referring to the band-pass-filter nature of this technique, it appears that as the detection scheme becomes exclusively a lower-frequency detection scheme, the number of negative events increases. Hence, to detect more representative negative events near the floor (that is, more common) a longer short-time-variance period should be used, such as $T^*_{\rm ST} = 1.0$, whereas it appears that a dimensionless period of 0.2 would most nearly represent the true character of a positive mass-flux event near the floor.

Figures 11 and 12 illustrate the optimum conditionally averaged positive and negative mass-flux events for three positions in the boundary layer. For both the positive and negative events a threshold of 0.8 was acceptable. The short-time-variance periods were based upon the results given in figure 10 for $y/\delta = 0.3$ and were chosen to be $T^*_{\rm ST} = 0.2$ for the positive event and $T^*_{\rm ST} = 1.0$ for the negative event.

From figures 11 and 12, it is clear that the typical positive mass-flux event is stronger and more energetic than the typical negative event since its peak-to-peak value is much greater. It can also be seen that the 'wave front' of the positive event is steeper than for the negative event, again showing that the positive event contains higher-frequency motions. If the negative event was deduced using the same short-time-variance period as for the positive event, an event would result that is of the same magnitude and shape as the positive event (but inversely symmetric). However, the number of individual realizations would be so small as to make the event atypical. The same is true for the positive event being deduced using the same short-time-variance period as the negative event; the number of individual events would be minimal.

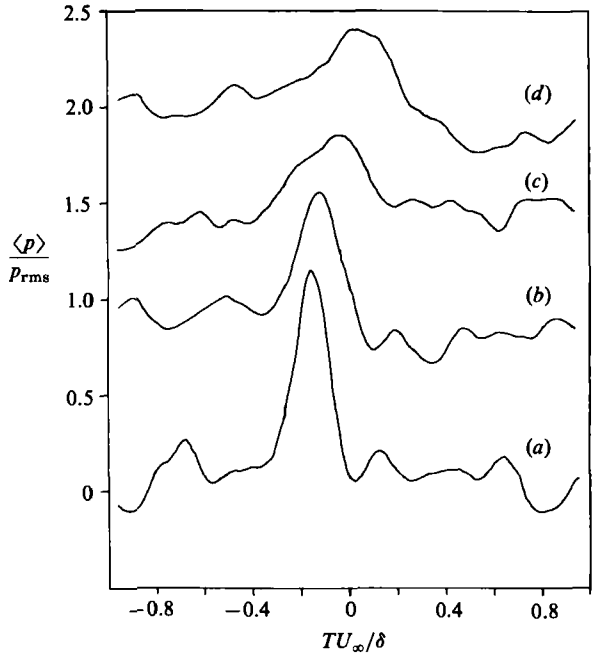

FIGURE 13. Average pressure events conditioned upon the positive mass-flux events at different heights: hot-wire located 0.09 downstream of pressure transducer; detection wire located at (*a*) $y/\delta = 0.03$, (*b*) 0.13, (*c*) 0.22, (*d*) 0.30; $T^*_{\rm ST} = 0.2$, $k = 1.2$.

5.3. *Pressure–mass flux two-point conditioning*

Two-point conditional sampling was performed on the data taken with a single normal hot wire and a wall-pressure transducer. At all times, the short-time variance of the mass-flux signal was used as the detection signal. When an event was detected in the mass-flux signal, the wall pressure was sampled simultaneously.

The height and streamwise extent of the organized structures was investigated by placing the hot wire directly downstream of the wall-pressure transducer at four different heights in the boundary layer. For a streamwise hot-wire/pressure-transducer separation of 0.09δ, figure 13 shows the average positive conditioned wall-pressure events for each of the y/δ-values of the hot wire. Each of these pressure events was found by conditioning upon the mass-flux events ($k = 0.8$, $T^*_{\rm ST} = 0.2$) whose average is similar to that seen in figure 11.

The main feature to note is the clear average pressure event that is extracted by conditioning upon the mass-flux signal; this is best illustrated at $y/\delta = 0.03$. This average event is almost as large as when the pressure was conditioned upon itself, although slightly different in shape. The difference in shape occurs because, in the latter case, all pressure events were summed about a point on the steep rise, accentuating that part of the event and neglecting the downside of the peak. This deduced pressure event agrees with the suggestion of a symmetric event made in §5.1. While the structure deteriorates slightly as y/δ increases, the strong similarity between events at different y/δ-values indicates an organized structure of significant height (at least 0.3δ).

Similarly to figure 13, figure 14 shows the average pressure events (conditioned upon the mass flux) for a streamwise separation of 1.41δ and for four heights of the

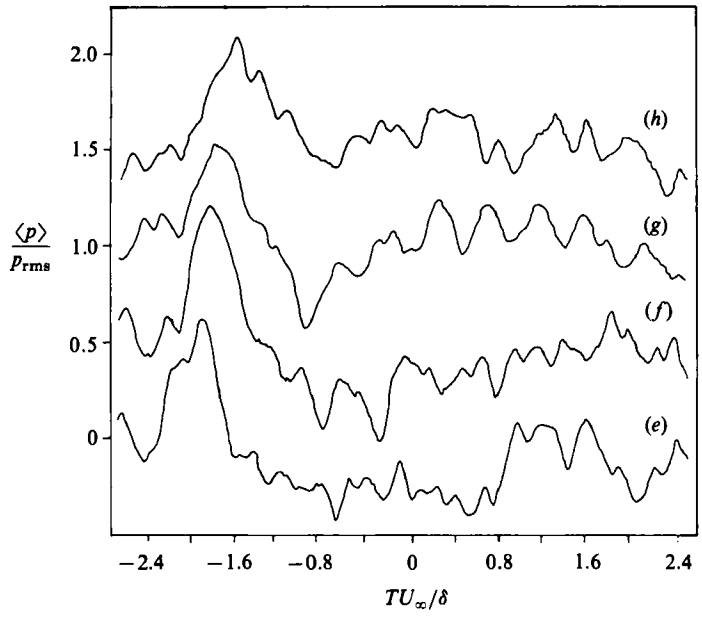

FIGURE 14. Average pressure events conditioned upon the positive mass-flux events at different heights: hot-wire located 1.41δ downstream of pressure transducer; detection wire located at: (*e*) $y/\delta = 0.03$, (*f*) 0.13, (*g*) 0.22, (*h*) 0.30; $T^*_{ST} = 0.2$, $k = 1.2$.

hot-wire. The persistence of clear pressure events above the background signal indicates that the organized structure has preserved its identity for almost one-and-a-half boundary-layer thicknesses downstream. This result based on ensemble-averaged events therefore complements the conclusion drawn in §4.2 on the basis of cross-correlation methods, and the VITA technique supports the notion of strong streamwise structure coherence.

The spanwise extent of the structures was explored by introducing a spanwise separation between the hot wire and the pressure transducer. Again, the conditional-sampling results reinforced the conclusions of §4.2 that the large-scale structures have a very limited spanwise extent.

5.4. *Three-point mass flux*

Two-point conditional sampling was performed on data taken simultaneously by three hot-wires. The three wires were located at $y/\delta = 0.37$, 0.46 and 0.57 and the detection signal was the short-time variance of either the middle wire or the lowest wire. When an event was detected, all three signals were sampled simultaneously.

The three mass-flux signals and the short-time variance of the lowest wire are shown in figure 15 for $T^*_{ST} = 0.2$ and a threshold of 0.8. The similarity of the three mass-flux signals, especially in the proximity of detected events, is remarkable and gives a strong indication of an organized structure. The inclination of these structures, previously discussed in the context of the cross-correlation, is also evident here by the shifting of the peaks from position to position.

Figure 16 depicts the average positive events from the three wires, all conditioned upon the middle wire ($k = 0.8$, $T^*_{ST} = 0.2$). As expected, the average event from the conditioning signal is much more distinct than those events that are two-point

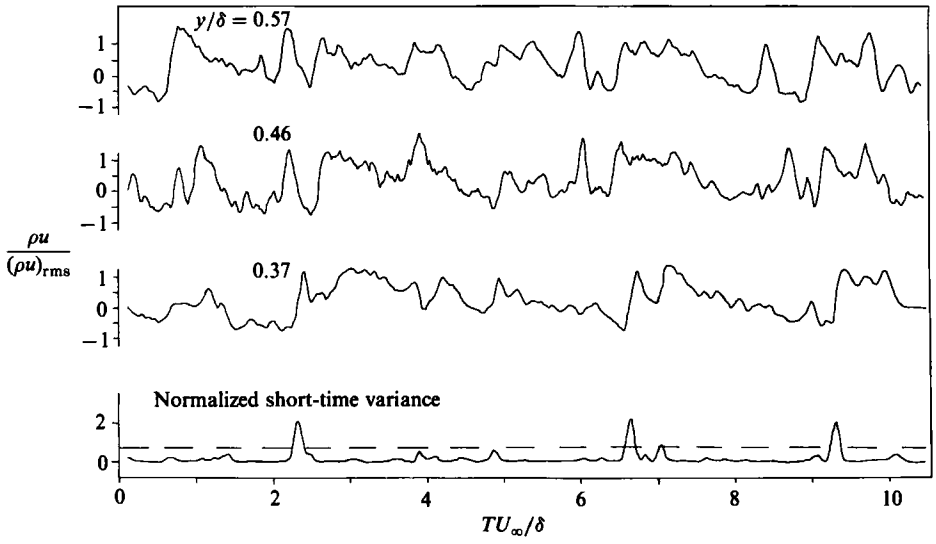

FIGURE 15. Three simultaneously measured, instantaneous mass-flux signals with a corresponding short-time-variance signal from the bottom hot wire. $T^*_{\rm ST} = 0.2$.

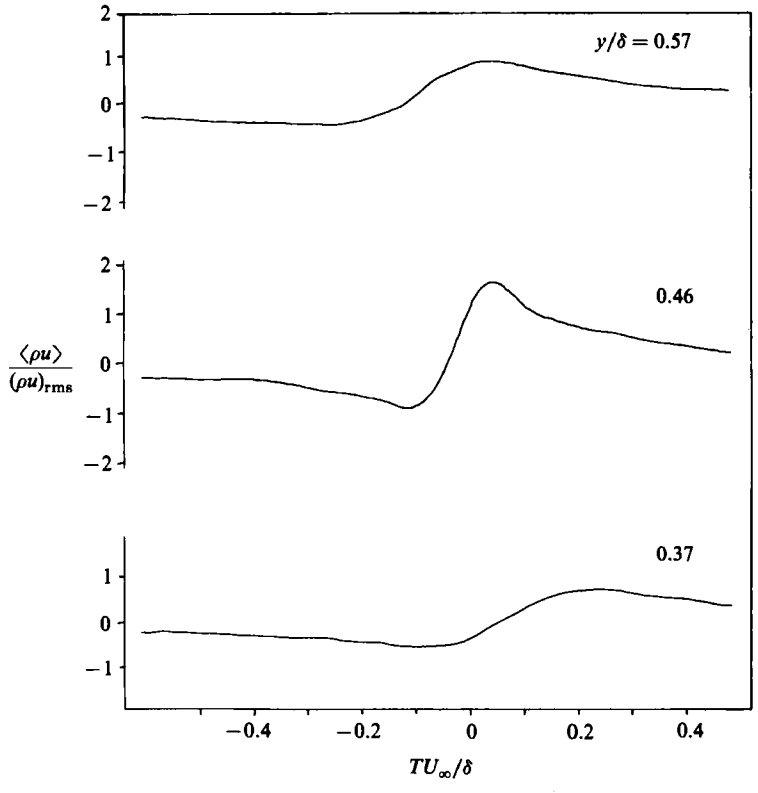

FIGURE 16. 'Optimized' average positive mass-flux events from the three-wire probe. Signals conditioned upon the middle wire. $T^*_{\rm ST} = 0.2$, $k = 0.8$.

conditioned averages. However, the existence of an average organized structure spanning the distance between the three wires is clearly indicated.

An average structure angle can also be determined from the average positive events by using the time delay between the points where each event crosses zero during its steep rise. The angles that result (45° from bottom to middle, 63° from middle to top, and 51° from bottom to top) are very similar to those deduced from the cross-correlation.

5.5. *Instantaneous-structure-angle determination*

The average structure-angle measurements reported here and elsewhere are very useful in describing the overall large-scale structure of the boundary layer. However, the key to a physical understanding of these structures lies with the instantaneous behaviour, not the average. To determine the instantaneous structure angles, a sampling technique was devised for the mass-flux fluctuations from the dual hot-wire probe (fixed-wire separation of 0.09δ). The algorithm consists of six parts:

(i) Find regions of high turbulent activity by using the VITA technique to conditionally sample each signal separately ($k = 0.8$, $T^*_{ST} = 0.2$);

(ii) Set an 'event length' L which corresponds approximately to the period of the steep rise or fall of an individual event (from figure 8 this was found to be $L^* = LU_\infty/\delta = 0.3$);

(iii) Within a time window T_w look in the upper-wire signal for the event nearest each lower-wire event (T_w is set large enough that any further increase does not affect the output of the technique and only acute structure angles will be accepted. This results in a certain number of 'event pairs', less than the total number of VITA events for either wire, since not every event will have a 'neighbour' on the other wire within T_w. The value of T_w used was $T^*_w = T_wU_\infty/\delta = 0.4$);

(iv) Find the time separation between each pair of events by using the local maximum of the short-time variance as a reference point;

(v) Compute the short-term correlation between each pair:

$$R_{12}(s)|_{ST} = \left(\frac{1}{\hat{\sigma}_1\,\hat{\sigma}_2}\right)\frac{1}{L}\int_{-\frac{1}{2}L}^{+\frac{1}{2}L} y_1(t)\,y_2(t+s)\,\mathrm{d}t,$$

where y_1 is the lower-wire mass flux, y_2 is the upper-wire mass flux, $\hat{\sigma}_1$ is the short-time r.m.s. of y_1 over period L, and $\hat{\sigma}_2$ is the short-time r.m.s. of y_2 over period L. The correlation time delay s is allowed to vary by $\pm\frac{1}{2}L$ so that the true phase relationship between each pair of events can be found;

(vi) If the maximum value of the short-term cross-correlation (corresponding to s_{max}) exceeds 0.90, the pair is accepted as representing a single large-scale structure. The actual delay time is then found by adding s_{max} to the time separation found in step (iv). This total delay time is used along with the wire separation distance and the local mean velocity (as in §4.1) to give an instantaneous structure angle.

In summary, the technique searches for highly correlated, highly energetic events occurring in both signals 'near-simultaneously', and deduces an instantaneous structure angle from their separation time. It should be noted that this method is not dependent on the VITA technique *per se*; any conditional-sampling technique could be used to find the energetic portions of each signal.

To achieve a sufficient number of realizations of the instantaneous angles, data records four times as long as usual were analysed (i.e. 98304 data points instead of 24576). The number of accepted pairs was approximately 60 % of the number of VITA

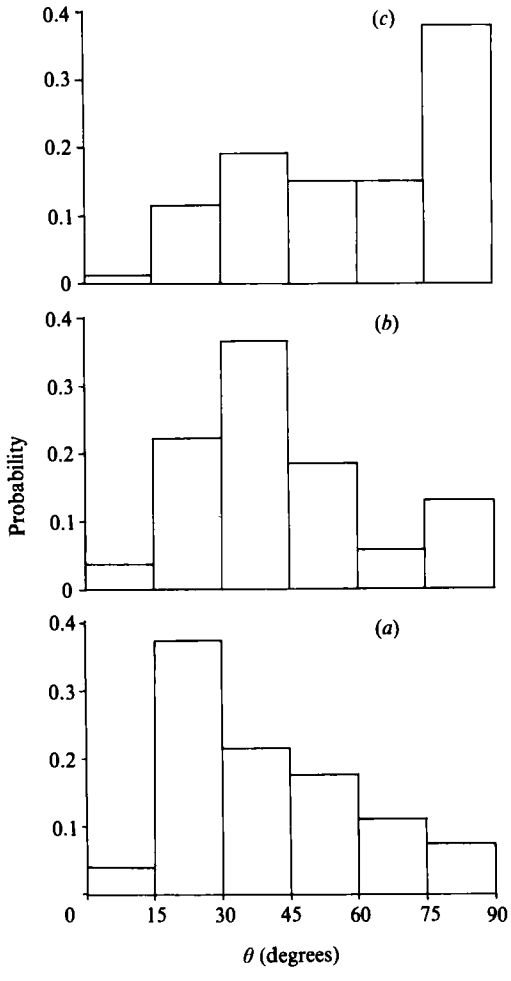

FIGURE 17. Probability distribution of instantaneous structure angles: (*a*) $y/\delta = 0.1$, 115 events; (*b*) $y/\delta = 0.3$, 306 events; (*c*) $y/\delta = 0.9$, 75 events.

events. The first point of note is that the average value of the instantaneous angle matched the mean structure angle very well. The values at the wall were slightly higher than in figure 5, but the distribution through the rest of the boundary layer was virtually identical. The standard deviation of the instantaneous angles was computed to be 20° throughout most of the boundary layer, indicating a large spread in the inclination of the structures. A histogram was computed and is shown in figure 17 (*a*, *b*, *c*) for three points in the boundary layer. Near the floor, the majority of the structures have an angle below 45°, with the most populated state being 15–30°, and very few structures with an angle of 90°. Away from the wall ($y/\delta = 0.3$), the structures shift towards 45° with an increased population at 90°. At the edge of the boundary layer ($y/\delta = 0.9$) the population between 75–90° has increased dramatically, and it becomes dominant.

These trends can be interpreted in terms of the hairpin model of wall turbulence. In this model, the characteristic structures in the boundary layer are hairpin loops, and hairpins of all sizes populate the boundary layer. A typical hairpin vortex (see,

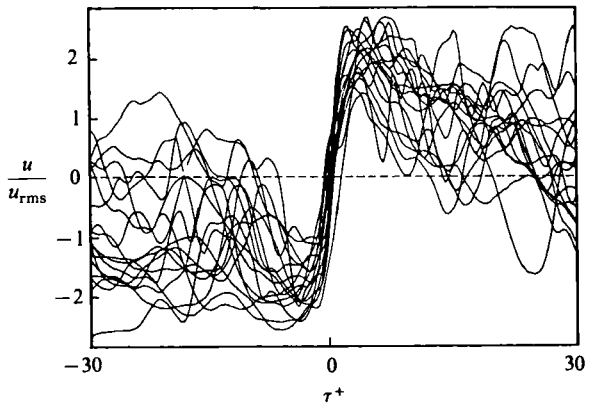

FIGURE 18. Individual streamwise velocity events detected by the VITA technique at $y^+ = 13$ (Alfredsson & Johansson 1982).

for example, Smith 1984) consists of elongated legs at the floor, a central portion inclined at 45°, and an upturned head at 90°. If the instantaneous-angle distribution were measured in this artificial boundary layer, the range of structure angles near the wall would vary from 0 to 90°, with the lower angles dominating since the mid- to large-scale structures would not display high angles near the wall. Away from the wall, the angle of the central portion would dominate, with a slightly higher population near 90° owing to the upturned heads of the structures of that size. Finally, near the edge of the boundary layer, the dominant angle would be close to 90°, since nearly all structures extending to that height would have upturned heads by that point. The distributions described for this idealized case of a 'forest' of hairpin loops are similar to those seen in figure 17, suggesting that the large-scale structures found in this compressible flow are consistent with this hairpin-structure interpretation.

6. Discussion and conclusions

6.1. *Final discussion*

It appears that the effect of compressibility on the large-scale motions is very small. Certainly, there are more similarities than differences between the events found in this compressible flow and those observed in incompressible boundary layers. For example, the deduced structure angles from this investigation are consistent with Head & Bandyopadhyay's (1981) observations in incompressible flow. The eddy angle is low near the floor, increases quickly to 45° (where it remains throughout 70% of the boundary layer), and increases again near the edge of the boundary layer.

The measurements in fully developed turbulent water-channel flows by Johansson & Alfredsson (1982) using VITA conditional sampling also show a strong similarity to the present results. Figure 18 shows a number of individual positive streamwise velocity events from their flow. Qualitatively, this figure compares quite favourably to figure 8, which shows individual positive mass-flow events from this investigation. Both figures show the individual events possessing a uniform steep rise and having a higher level at the end of the event than the beginning. In addition, the average amplitude of the events in both cases seems to be approximately four times the r.m.s. level. Finally, the ensemble-averaged positive velocity events detected in

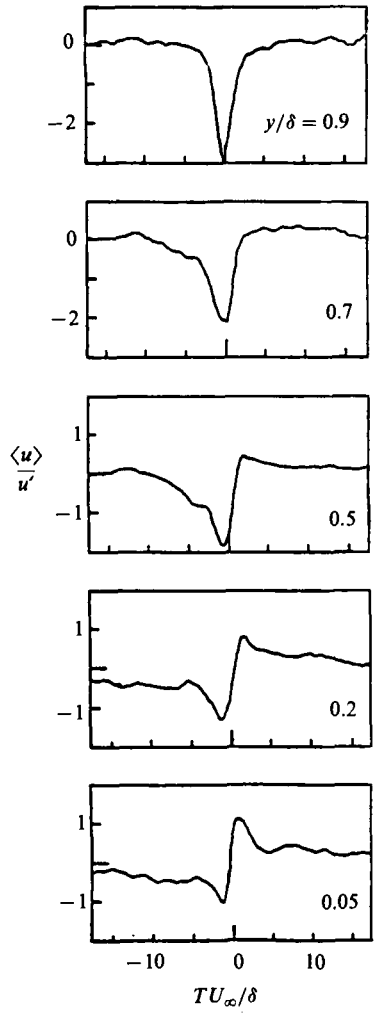

FIGURE 19. Ensemble-average time histories of the conditionally sampled streamwise velocity. Detection is based on a smoothed rectified high-frequency u-component at each y-value (Thomas & Bull 1983).

incompressible flows by Thomas & Bull (1983) were found to be strikingly similar to the mass-flow events from this investigation (figure 11). Thomas & Bull (1983) performed extensive measurements, from $y/\delta = 0.05$ to 0.91, as seen in figure 19. The character of their average event changes (with increasing height in the boundary layer) in a manner similar to that of the compressible flow investigated here. As the distance from the wall increases, the drop prior to the steep rise becomes more significant in both cases.

6.2. *Conclusions*

This experimental investigation of a compressible flow found that large-scale structures, inclined at 45° to the wall, appear to fill the major extent of the boundary layer. As they convect downstream, these structures retain much of their shape and character, and preserve their identity for at least 1.5δ. However, the spanwise extent of the structures is very limited. The average and the instantaneous behaviour of

these structures was found to be consistent with a distribution of hairpin vortex loops. Furthermore, this investigation indicates that the effect of compressibility on large-scale organized structures in an undisturbed turbulent boundary layer is small.

This work was supported by AFOSR Grant 85-0126, monitored by Dr James McMichael.

REFERENCES

BLACKWELDER, R. F. & KAPLAN, R. E. 1976 On the wall structure of the turbulent boundary layer. *J. Fluid Mech.* **76**, 89.

BOGARD, D. G. & TIEDERMAN, W. G. 1986 Burst detection with single-point velocity measurements. *J. Fluid Mech.* **162**, 389.

BROWN, G. L. & THOMAS, A. S. W. 1977 Large structure in a turbulent boundary layer. *Phys. Fluids* **20**, 243.

CHEN, C. P. & BLACKWELDER, R. F. 1978 Large-scale motion in a turbulent boundary layer: a study using temperature contamination. *J. Fluid Mech.* **89**, 1.

DECKKER, B. E. L. 1980 An investigation of some unsteady boundary layers by the schlieren method. *Intl Symp. on Flow Visualization, Ruhr-Universität.*

DECKKER, B. E. L. & WEEKES, M. E. 1976 The unsteady boundary layer in a shock tube. *Proc. Instn Mech. Engrs* **190**, 287.

DUSSAUGE, J. P. & GAVIGLIO, J. 1981 Bulk dilatation effects on Reynolds stress in the rapid expansion of a turbulent boundary layer at supersonic speed. *Proc. Third Symp. on Turbulent Shear Flows, Univ. California, Davis.*

FERNHOLZ, H. H. & FINLEY, P. J. 1980 A critical commentary on mean flow data for two-dimensional compressible turbulent boundary layers. *AGARDograph* No. 253.

HANLY, R. D. 1975 Effects of transducer flushness on fluctuating surface pressure measurements. *AIAA Paper* 75-534.

HEAD, M. R. & BANDYOPADHYAY, P. 1981 New aspects of turbulent boundary-layer structure. *J. Fluid Mech.* **107**, 297.

JAYARAM, M., TAYLOR, M. W. & SMITS, A. J. 1987 The response of a compressible turbulent boundary layer to short regions of concave surface curvature. *J. Fluid Mech.* **175**, 343.

JOHANSSON, A. V. & ALFREDSSON, P. H. 1982 On the structure of turbulent channel flow. *J. Fluid Mech.* **122**, 295.

KLINE, S. J., CANTWELL, B. J. & LILLEY, G. M. 1981 *Proc. 1980–81 AFOSR-HTTM Stanford Conf. on Complex Turbul. Flow: Comparison of Computation and Experiment*, Vol. 1. Thermo Sci. Div., Stanford University, Stanford, CA.

KLINE, S. J., REYNOLDS, W. C., SCHRAUB, F. A. & RUNSTADLER, P. W. 1967 The structure of turbulent boundary layers. *J. Fluid Mech.* **30**, 741.

KOVASZNAY, L. S. G. 1950 The hot-wire anemometer in supersonic flow. *J. Aero. Sci.* **17**, 565.

MOIN, P. & KIM, J. 1985 The structure of the vorticity field in turbulent channel flow. Part 1. Analysis of instantaneous fields and statistical correlations. *J. Fluid Mech.* **155**, 441.

MORKOVIN, M. V. 1962 Effects of compressibility on turbulent flows. *Int. Symp. on the Mechanique de la Turbulence*, p. 367. Centre National de la Recherche Scientifique, Paris.

OFFEN, G. R. & KLINE, S. J. 1974 Combined dye streak and hydrogen bubble visual observations of a turbulent boundary layer. *J. Fluid Mech.* **62**, 223.

OFFEN, G. R. & KLINE, S. J. 1975 A proposed model of the bursting process in turbulent boundary layers. *J. Fluid Mech.* **70**, 209.

OWEN, F. K. & HORSTMAN, C. C. 1972 On the structure of hypersonic turbulent boundary layers. *J. Fluid Mech.* **53**, 611.

OWEN, F. K. & HORSTMAN, C. C. 1981 Turbulent measurements in an equilibrium hypersonic boundary layer. *AIAA Paper* 74-93.

OWEN, F. K., HORSTMAN, C. C. & KUSSOY, M. I. 1975 Mean and fluctuating flow measurements of a fully-developed, non-adiabatic, hypersonic boundary layer. *J. Fluid Mech.* **70**, 393.

RAJAGOPALAN, S. & ANTONIA, R. A. 1979 Some properties of the large structure in a fully developed turbulent duct flow. *Phys. Fluids* **22**, 614.

ROBINSON, S. K. 1985 Instantaneous velocity profile measurements in a turbulent boundary layer. *Chem. Engng Commun.* **43**, 347.

ROBINSON, S. K. 1986 Space–time correlation measurements in a compressible turbulent boundary layer. *AIAA Paper* 86-1130.

SETTLES, G. S. 1975 An experimental study of compressible turbulent boundary layer separation at high Reynolds number. Ph.D. thesis, Mechanical and Aerospace Engineering Department, Princeton University.

SMITH, C. R. 1984 A synthesized model of the near-wall behavior in turbulent boundary layers. In *Proc. Eighth Symposium on Turbulence* (ed. G. K. Patterson & J. L. Zakin), Department of Chemical Engineering, University of Missouri-Rolla.

SMITS, A. J., HAYAKAWA, K. & MUCK, K. C. 1983 Constant-temperature hot-wire anemometer practice in supersonic flows. Part I – The normal wire. *Exp. Fluids.*

SMITS, A. J. & MUCK, K. C. 1987 Experimental study of three shock wave/turbulent boundary layer interactions. *J. Fluid Mech.* **182**, 291.

SPINA, E. F. & SMITS, A. J. 1986 Organized structures in a supersonic, turbulent boundary layer. *MAE Rep.* 1736. Princeton University.

SUBRAMANIAN, C. S., RAJAGOPALAN, S., ANTONIA, R. A. & CHAMBERS, A. J. 1982 Comparison of conditional sampling and averaging techniques in a turbulent boundary layer. *J. Fluid Mech.* **123**, 335.

TAYLOR, M. W. 1984 A supersonic turbulent boundary layer on concavely curved surfaces. M.S.E. thesis, Mechanical and Aerospace Engineering Department, Princeton University.

THOMAS, A. S. W. & BULL, M. K. 1983 On the role of wall-pressure fluctuations in deterministic motions in the turbulent boundary layer. *J. Fluid Mech.* **128**, 283.

VAN DYKE, M. 1982 *An Album of Fluid Motion.* Stanford: Parabolic.

WYNGAARD, J. C. 1968 Measurements of small-scale turbulence with hot-wires. *J. Phys.* E: *Sci. Instrum.* **1**, 1105.